Monthly Notices
of the
ROYAL ASTRONOMICAL SOCIETY

MNRAS **449,** 1826–1833 (2015) doi:10.1093/mnras/stv425

Probing model interstellar grain surfaces with small molecules

M. P. Collings,[1] V.L. Frankland,[1,2] J. Lasne,[1,3] D. Marchione,[1] A. Rosu-Finsen[1⋆] and M. R. S. McCoustra[1]

[1]*Institute of Chemical Sciences, Heriot-Watt University, Edinburgh EH14 4AS, UK*
[2]*Department of Chemistry, University of Leeds, Leeds LS2 9JT, UK*
[3]*Laboratoire Interuniversitaire des Systèmes Atmosphériques (LISA), CNRS UMR 7583, Université Paris-Est Créteil, Université Paris Diderot, Faculté des Sciences et Technologie, 61 avenue du Général de Gaulle, F-94010 Créteil Cedex, France*

Accepted 2015 February 24. Received 2015 February 24; in original form 2014 December 05

ABSTRACT

Temperature-programmed desorption and reflection-absorption infrared spectroscopy have been used to explore the interaction of oxygen (O_2), nitrogen (N_2), carbon monoxide (CO) and water (H_2O) with an amorphous silica film as a demonstration of the detailed characterization of the silicate surfaces that might be present in the interstellar medium. The simple diatomic adsorbates are found to wet the silica surface and exhibit first-order desorption kinetics in the regime up to monolayer coverage. Beyond that, they exhibit zero-order kinetics as might be expected for sublimation of bulk solids. Water, in contrast, does not wet the silica surface and exhibits zero-order desorption kinetics at all coverages consistent with the formation of an islanded structure. Kinetic parameters for use in astrophysical modelling were obtained by inversion of the experimental data at sub-monolayer coverages and by comparison with models in the multilayer regime. Spectroscopic studies in the sub-monolayer regime show that the C–O stretching mode is at around 2137 cm^{-1} (5.43 μm), a position consistent with a linear surface–CO interaction, and is inhomogenously broadened as resulting from the heterogeneity of the surface. These studies also reveal, for the first time, direct evidence for the thermal activation of diffusion, and hence de-wetting, of H_2O on the silica surface. Astrophysical implications of these findings could account for a part of the missing oxygen budget in dense interstellar clouds, and suggest that studies of the sub-monolayer adsorption of these simple molecules might be a useful probe of surface chemistry on more complex silicate materials.

Key words: molecular data – molecular processes – methods: laboratory: molecular – dust, extinction.

1 INTRODUCTION

The gas–grain interaction is increasingly recognized as central to the physics and chemistry of the interstellar medium (ISM; Williams & Taylor 1996; Garrod et al. 2006; Dulieu et al. 2013). Such heterogeneous interactions rest upon fundamental aspects of the gas–solid interaction such as the nature of surface binding sites, binding energies in those sites and rates of surface diffusion. The composition of the interstellar gas is well described (Tielens 2013), but the nature of the grain surface is less well understood. We know from depletion studies that both solid carbonaceous and silicaceous materials are likely to exist (Tielens 2005), with evidence from mid- (Tielens 2005) and far-IR (Onaka & Okada 2003) spectroscopic observations pointing towards the silicate materials coming from the iron-magnesium silicate family and exhibiting both amorphous and crystalline morphologies. The recent recovery of interstellar grains by the Stardust Mission tentatively confirms this hypothesis (Westphal et al. 2014). In this work, amorphous silica is used as a simple model for the more complex silicate materials to demonstrate the potential for utilizing simple gases to learn more of the nature of the gas–grain interaction.

As to the gas itself and the choice of probe species, atomic oxygen and nitrogen are among the most abundant elements observed in the ISM, with respective abundances of 3×10^{-4} and 7.5×10^{-5} relative to H measured in diffuse clouds (Meyer, Cardelli & Sophia 1997; Meyer, Jura & Cardelli 1998). Despite these apparently low concentrations, a range of O and N bearing species have been observed in the ISM. Among them, molecular oxygen (O_2), carbon monoxide (CO) and molecular nitrogen (N_2) are predicted to be among the most abundant small molecules in dense cores, suggesting that these species contain a considerable proportion of the O, C and N budgets; while water (H_2O) is the most abundant ice component in such environments (Ehrenfreund &

⋆ E-mail: ar163@hw.ac.uk

Charnley 2000). Although the observed concentrations of most species, such as CO, agree well with the values predicted by gas-phase chemistry, the models are unable to explain the formation and abundance of several essential molecules, including O_2, N_2 and H_2O.

CO has been detected in dense molecular clouds both in the gas phase and in the icy mantles coating interstellar dust grains (Chiar et al. 1998; Pontoppidan et al. 2003; Thi et al. 2010) with abundances of up to 10^{-4} (see e.g. Chiar et al. 1998; Pontoppidan et al. 2003; Pontoppidan, van Dishoeck & Dartois 2004), and also in diffuse clouds (Liszt 2007). Since N_2 is infrared inactive and radio quiet, its abundance has been inferred through the detection of the gaseous N_2H^+ ion, which is formed by the H_3^+ proton transfer reaction with N_2. The calculated gas-phase abundance of N_2 from N_2H^+ can reach a few times 10^{-5} in diffuse clouds (van Dishoeck et al. 1992; Bergin et al. 2002), whilst in the cold and dense cores, it decreases by at least a factor of 2 (Belloche & Andre 2004). The results from the Odin and the submillimeter wave astronomy satellite missions placed an upper limit on the gaseous O_2 abundance in dense clouds as 3–10 $\times$ 10^{-8} (Goldsmith et al. 2000; Larsson et al. 2007; Sandqvist et al. 2008; Liseau et al. 2012). As a dense cloud forms from the gravitational collapse of a diffuse cloud, the origin of the apparent reduction of the total O budget observed (from $[O] = 3 \times 10^{-4}$ in diffuse clouds to $[O_2] = 3$–10×10^{-8} in dense cores) is unclear. Moreover, the observed O_2 concentration is several orders of magnitude lower than predicted from gas-phase chemistry models (Hollenbach et al. 2009; Liseau et al. 2012). The main theory about this missing oxygen relates to the gas-phase reactions, and particularly the formation of CO; however, the observed cumulated abundance of all O-bearing species does not match the initial atomic abundance (Whittet 2010). Another suggestion is that the missing oxygen is carried by O-bearing carbonaceous molecules present in the icy mantle of the dust grains. Recent gas–grain chemical models have demonstrated that the low abundance of O_2 can be obtained in dark cloud environments (Hincelin et al. 2011) based on the fresh insights into elemental oxygen depletion (Jenkins 2009; Whittet 2010). This indicates that the chemical models need to include adsorption and desorption processes on interstellar dust grains to match the observed molecular abundances.

Interstellar H_2O has been studied extensively (Gillet & Forrest 1973; Bar-Nun et al. 1985; O'Neill & Williams 1999; Collings et al. 2003b and 2004; Tielens 2013 and references therein), which is mainly detected in the solid state on the 3.07 μm O–H stretching absorption band. When H_2O is deposited onto a dust grain at low temperatures, about 10 K, it is believed to do so by ballistic deposition. The incoming H_2O molecules 'hit and stick' to the surface leading to a microporous, amorphous H_2O ice (Stevens et al. 1999). Warming of the H_2O ice at 38–68 K leads to the collapse of the pores to form high density, non-porous amorphous H_2O; this phase change is not apparent in infrared spectroscopy, but can be detected through various other analytical techniques (Narten, Venkatesh & Rice 1976; Jenniskens & Blake 1994; Lu et al. 2001). Further annealing leads to the formation of the cubic crystalline phase above 140 K (Jenniskens et al. 1995; Smith et al. 1997).

With the goal of developing our understanding of the gas–grain interaction, we will focus our efforts on the interactions of the diatomic species (CO, N_2 and O_2) and H_2O with our model silicate surface. Temperature-programmed desorption (TPD) will be used to characterize the binding energies of molecules with the model silicate surface, while reflection-absorption infrared spectroscopy (RAIRS) will be used to explore their binding sites and surface diffusion.

2 EXPERIMENTAL METHODS

The experiments were performed in an ultrahigh vacuum apparatus described in detail elsewhere (Fraser, Collings & McCoustra 2002). Briefly, the central chamber is evacuated with a diffusion pump to a base pressure of 2×10^{-10} mbar. The sample, an oxygen free high conductivity copper block coated with amorphous silica deposited by electron-beam evaporation of fused quartz silica (Thrower et al. 2009a), is mounted onto the end of a closed-cycle helium cooled cold finger. The silica substrate can be heated using a cartridge heater (Heatwave Labs, Inc.) situated behind the sample; the surface temperature is monitored by a KP-type (Au-Chromel) thermocouple. The chamber is equipped with a line-of-sight quadrupole mass spectrometer (QMS, Hiden Analytical Ltd, HAL301) for TPD and FTIR spectrometer (Varian 670-IR) and associated optics for RAIRS.

The films are deposited by background dosing of ultrapure gases onto the amorphous silica substrate held at 18 K. Exposures of the sample to the gas are expressed in monolayer (ML). TPD is performed by applying a heating ramp of 0.1–0.5 K s^{-1} to a suitable final surface temperature. The desorbing species are detected using the QMS. RAIRS is performed by co-addition of 512 scans recorded with a 75° grazing incidence to the normal of the surface and then collected by an mercury cadmium telluride detector cooled with liquid nitrogen. These experiments were conducted with a resolution of 1 cm^{-1}. All spectra were taken at a base temperature after annealing the film to the temperatures stated in the relevant figures.

3 RESULTS AND DISCUSSION

Figs 1(A–H) present the raw TPD profiles of background dosed O_2, CO, N_2 and H_2O desorbing from amorphous silica; the left-hand panel focuses on high coverages, and the right-hand panel shows low coverages. At low coverage, the TPD traces of O_2, CO, N_2 exhibit coincident trailing edges; at high coverage, they have coincident leading edges. For these species, the TPD profiles of the intermediate coverages exhibit both coincident leading and trailing edges; this implies that desorption occurs from three-dimensional multilayer islands formed before the completion of a monolayer. As these transition stages between sub-ML and multilayer coverages are likely to follow a variable fractional kinetic order, they are not analysed in this study. Because the desorption behaviour changes with coverage, the results are presented in two distinct sets dedicated to the multilayer and sub-ML regimes. For the H_2O TPD profiles in Figs 1(G–H), a different behaviour is observed. Both low-coverage and high-coverage data show only evidence of zero-order desorption and are consistent with previous data on multilayers of H_2O even down to the characteristic feature arising from the amorphous to crystalline phase transition (Fraser et al. 2001; Smith et al. 2014). However, this observation is inconsistent with the work of Bolina, Wolff & Brown (2005), though the inconsistency may simply be due to differences in the substrates and experimental systems.

3.1 Multilayer desorption from amorphous silica

The experimental TPD profiles of high coverages of O_2, CO, N_2 and H_2O on amorphous silica are displayed in Figs 2(A)–(D), respectively, with open symbols. O_2 desorption starts at 25.4 K, and the maximum rate is reached between 28.1 K and 29.8 K, depending on the coverage. CO desorption occurs at lower temperature: it starts at 25.0 K, and peaks between 27.1 and

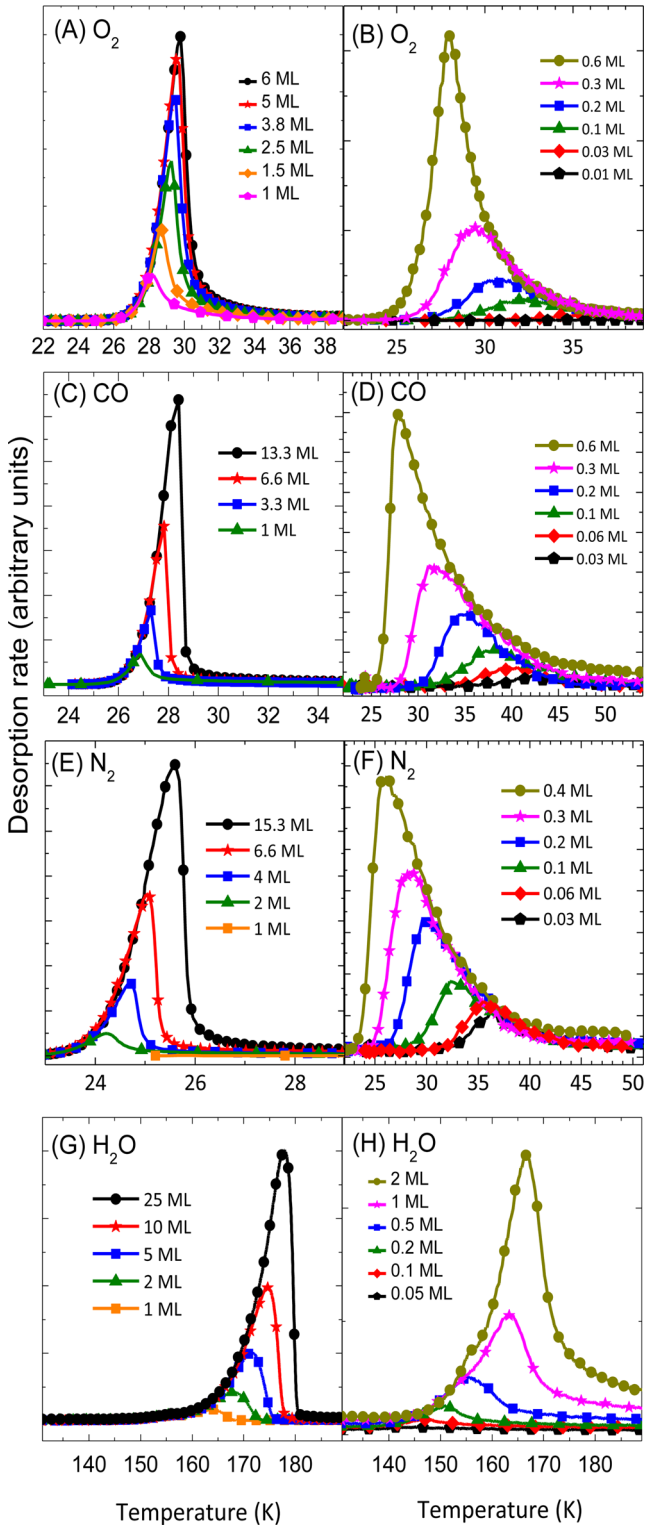

Figure 1. TPD profiles of (A-B) O_2, (C-D) CO, (E-F) N_2 and (G-H) H_2O on amorphous silica for high coverages on the left and low coverages on the right.

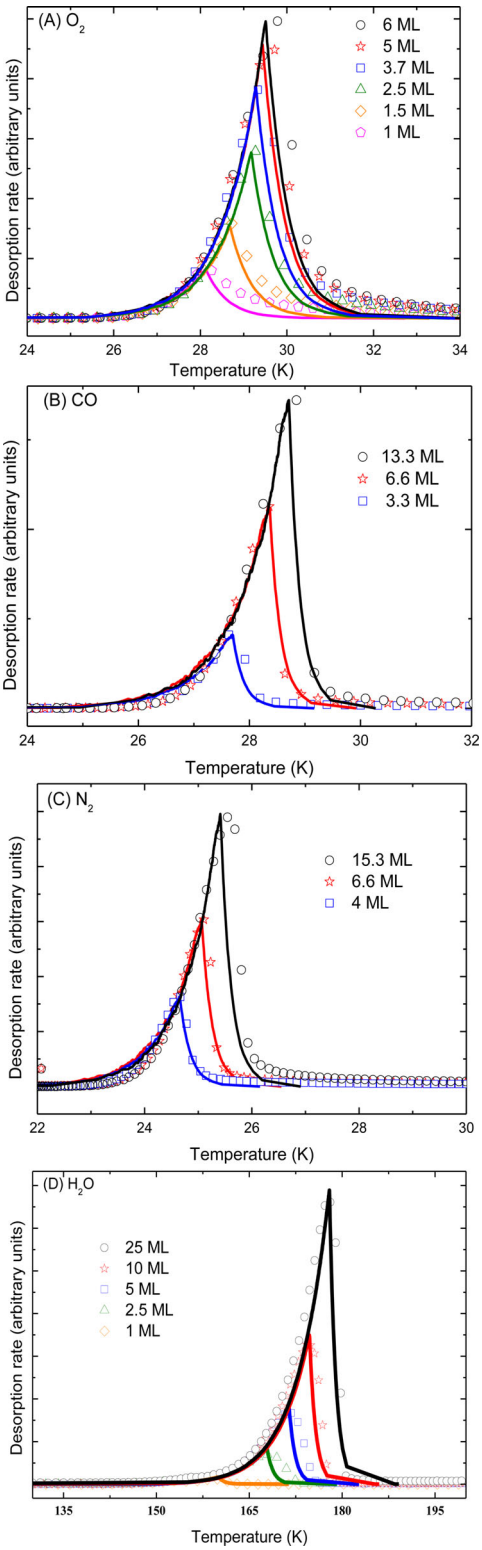

Figure 2. TPD profiles of (A) O_2, (B) CO, (C) N_2 and (D) H_2O multilayer desorption from amorphous silica (open symbols) and CKS fits (full lines) of the data.

28.8 K. N_2 begins to desorb at 22.0 K, with a peak between 24.2 and 25.6 K. H_2O desorption occurs at much higher temperature starting around 144 K, presenting the well-known feature due to crystallization at 150–155 K before reaching a maximum rate between 159 and 178 K. For each species, the profiles exhibit coincident leading edges, which is typical of zero-order desorption. This implies that the molecules are desorbing from the multilayer, where the lateral adsorbate–adsorbate interactions dominate.

To determine kinetic parameters for the multilayer desorption, leading edge analysis (King 1975) is combined with kinetic

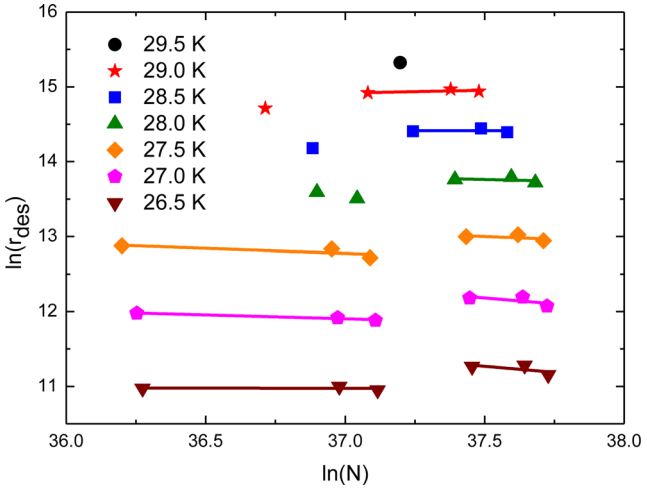

Figure 3. Leading edge analysis of the kinetic order of O_2 multilayer desorption from amorphous silica.

modelling using the Chemical Kinetic Simulator (CKS)[1] package. This approach has successfully been used to study the desorption kinetics of CO multilayers from water ice (Collings et al. 2003a) and C_6H_6 multilayers from amorphous silica (Thrower et al. 2009a). Leading edge analysis is based on the Polanyi–Wigner equation (1), which expresses the desorption rate $r_{\rm des}$ as function of $N(t)$ the surface concentration of the adsorbed species at time t:

$$r_{\rm des} = -\frac{dN}{dt} = \nu N\,(t)^n \exp\left[\frac{-E_{\rm des}}{k_{\rm B}T}\right], \quad (1)$$

where ν is the pre-exponential factor, n and $E_{\rm des}$ the desorption order and energy, $k_{\rm B}$ the Boltzmann constant and T the surface temperature. To determine $N(t)$, the initial concentration on the surface ($N_{\rm tot}$) is assumed to be equal to the rate of bombardment ($Z_{\rm W}$) multiplied by the dose time (τ) (equation (2)):

$$N_{\rm tot} = Z_W \tau = \frac{PS\tau}{\sqrt{2\pi m k_{\rm B} T}}, \quad (2)$$

where P is the pressure (in Pascal), S the sticking coefficient and m the mass of one of the molecules considered. If S is unity, then at the low surface temperatures employed in this study the desorption flux is negligible and all molecules are assumed to stick to the surface. The values of $N(t)$ are obtained by subtracting the total gas-phase concentration at the previous time step to the initial surface concentration ($N_{\rm tot}$).

The procedure for calculating the kinetic order of desorption (n) has been described elsewhere (Green et al. 2009). Briefly, the natural logarithm is applied to a rearranged version of the Polanyi–Wigner equation (1), giving, for fixed T, a linear relationship between $ln(r_{\rm des})$ and $ln(N)$, where the gradient equals n. Using this procedure leads to kinetic orders of $n = 0.03 \pm 0.06$ for CO and $n = 0.06 \pm 0.06$ for N_2. These are not inconsistent with the expected zero-order kinetics given the error limits derived from our analysis. Fig. 3 shows the relevant plot of $ln(r_{\rm des})$ against $ln(N)$ for the 1 to 6 ML O_2 TPD experiments. Here a cursory analysis might suggest a non-zero order of around 0.23 ± 0.11. However, on careful review of the data and a deeper investigation of the behaviour of O_2, we are led to the conclusion that the data in Fig. 3 present two regions of zero-order behaviour offset in terms of exhibiting different desorption rates and reflecting the $\alpha \rightarrow \beta$ phase transition in solid O_2 reported by Cairns & Pimentel (1965) and Freiman & Jodl (2004) and references therein at around 24 K. As the $\alpha \rightarrow \beta$ phase transition occurs, a monoclinic distortion in the crystal structure happens. However, a consensus about exactly what takes place at this transition has so far not been reached (Freiman & Jodl 2004 and references therein). Fortuitously, the experimental conditions of this work allows for the observation of this phase change through the different zero-order desorption regions. The same cannot be said for N_2 and CO. In these systems, the $\alpha \rightarrow \beta$ phase change is found to occur at higher temperatures, about 36 and 61 K, respectively, for N_2 and CO, and hence only observed at higher pressures (Gill & Morrison 1966; Freiman & Jodl 2004).

CKS is a stochastic integration program which integrates a raw law equation for each step in a reaction mechanism. A simple mechanism is used for the desorbing species (hereafter denoted as D):

$$D_{\rm ads} \rightarrow D_{\rm gas} \quad (3)$$

$$D_{\rm gas} \rightarrow D_{\rm pump}, \quad (4)$$

where $D_{\rm ads}$ indicates a molecule adsorbed on the surface, $D_{\rm gas}$ in the gas phase and $D_{\rm pump}$ a molecule removed from the system by pumping. In the simulations, the initial surface concentration is taken as $N_{\rm tot}$ and the values of ν and $E_{\rm des}$ for (3) are those obtained from leading edge analysis. The pumping step shown in (4) is assumed to be temperature independent and its rate coefficient (k) is obtained by comparing the experimental and simulated trailing edges for each dose. The resulting CKS fits are displayed with full lines in Figs 2(A–D) and describe the experimental data (open symbols) well. The average values of the kinetic parameters are presented in Table 1, these values are consistent with those found by other multilayer studies done on these molecules (Fraser et al. 2001; Haq, Harnett & Hodgson 2002; Collings et al. 2003a; Öberg et al. 2005; Bisschop et al. 2006; Fuchs et al. 2006; Acharyya et al. 2007; Noble et al. 2012). In the case of O_2, it is necessary to consider the $\alpha \rightarrow \beta$ phase transition and parallel desorption from the two phases. However, CKS modelling suggest a negligible effect of the phase transition on the empirically observed TPD profiles.

Although our analysis is consistent with the literature, there is some evidence for small deviations from zero-order behaviour as the rate of desorption approaches its maximum. This kind of behaviour has been investigated numerically in recent studies of methanol, ethanol and water desorption from graphene (Smith et al. 2014). Deviations from zero order as small as 0.05 have an impact on the shape of the TPD curve at its maximum. Our small deviation from zero and realistic 2σ error limits suggest that the three species are indeed expressing zero-order desorption. The small deviations may then reflect the impact of the surface heterogeneity in the final stages of multilayer desorption.

3.2 Sub-monolayer desorption from amorphous silica

The experimental TPD profiles of O_2, CO, N_2 and H_2O in the sub-ML regime on bare silica are presented in Figs 1(B), (D), (F) and (H), respectively, with full symbols. From this figure, the diatomic molecules present distinctively different behaviour to that of H_2O in this coverage range.

[1] Chemical Kinetics Simulator (CKS), Version 1.0, IBM, IBM Almaden Research Centre, 650 Harry Road, Mailstop ZWX1D1, San Jose, CA, USA. Further information may be obtained from http://www.almaden.ibm.com/st/computational_science/ck/?cks

Table 1. Average kinetic parameters for multilayer coverages of O_2, CO, N_2 and H_2O desorbing from amorphous silica. [1] = Acharyya et al. (2007); [2] = Fuchs et al. (2006); [3] = Fraser et al. (2001).

Species	n	ν / molecules cm^{-2} s^{-1} (this work)	E_{des} /kJ mol^{-1} (K) (this work)	E_{des} / kJ mol^{-1} (literature)
O_2	-0.07 ± 0.07	10^{28}	7.5 ± 0.2 (902 ± 24)	7.6 ± 0.2 (914 ± 24) [1,2]
	-0.13 ± 0.24			
CO	0.03 ± 0.6	10^{26}	7.3 ± 0.3 (878 ± 36)	7.1 ± 0.2 (854 ± 24) [1,2]
N_2	0.06 ± 0.06	10^{27}	6.9 ± 0.3 (830 ± 36)	6.6 ± 0.2 (794 ± 24) [2]
H_2O		10^{28}	49.3 ± 2 (5930 ± 240)	48 ± 0.5 (5770 ± 60) [3]

In the case of O_2, CO and N_2, the TPD traces exhibit coincident trailing edges, which is usually typical of second-order recombinative desorption. However, these species do not dissociate on silica at low temperature. Instead, the amorphous silica surface presents a range of binding sites with different binding energies for adsorption (Thrower et al. 2009a). The alignment of the trailing edges indicates that the molecules are mobile enough to find the deepest, energetically most favourable binding sites on the amorphous silica surface. As a consequence, the molecules situated in the weaker binding sites desorb first, resulting in desorption peak broadening.

Since the assumption of a single value for E_{des} is no longer valid, leading edge analysis cannot be applied to the sub-ML coverages desorbing from amorphous silica. Instead, direct inversion of the Polanyi–Wigner equation (5) gives E_{des} as function of the surface concentration at time t, $N(t)$:

$$E_{des} = -k_B T \ln\left(\frac{dN/dt}{\nu N(t)^n}\right) \quad (5)$$

This technique was first reported by Tait et al. (2005) and has since been adapted to describe small molecule desorption from similar heterogeneous surfaces (Thrower et al. 2009b). The values of dN/dt are calculated as in the multilayer case, and n and ν are assumed as 1 and 1×10^{12} s^{-1}, respectively. The latter is typical of the pre-exponential factor for desorption of a van der Waals bound adsorbate. The values of $N(t)$ are determined from N_{tot} using the same procedure as discussed for the leading edge analysis. Plots of E_{des} against $N(t)$ are constructed for each O_2 sub-ML dose (Fig. 4(A)). Similar plots have been constructed for CO and N_2 but are not presented here. An exponential fit is then made to the data to obtain the $E_{des}(N_{ads})$ function (an example is shown in Fig. 4(A) for the 0.3 ML dose). The kinetic modelling technique used is based on the FORTRAN 90 program developed to model C_6H_6 desorption peaks in the work of Thrower et al. (2009c). The experimental time and surface temperatures are taken as an input and the program coding altered for each E_{des} function (the exponentials extracted from the fits mentioned above) to calculate the desorption rate through the Polanyi–Wigner equation (1). The output data contain the calculated desorption rate and value of E_{des} at each simulated time point. The simulations are displayed in Fig. 4(B) with full lines and agree well with the experimental data, indicating that the desorption of the O_2, CO and N_2 sub-MLs from silica follows first-order kinetics with a range of desorption energies; the calculated values of which are displayed in Table 2.

For the H_2O data, the leading edge coincidence and the consistency throughout the sub-ML to multilayer TPD data suggest that even at the lowest coverages H_2O is found on the surface as clusters or islands. The low-coverage phase therefore exists as an equilibrium between a gas and a condensed phase. Under such conditions, zero-order desorption is expected and is observed. This arises simply as a consequence of the balance of intermolecular forces at play.

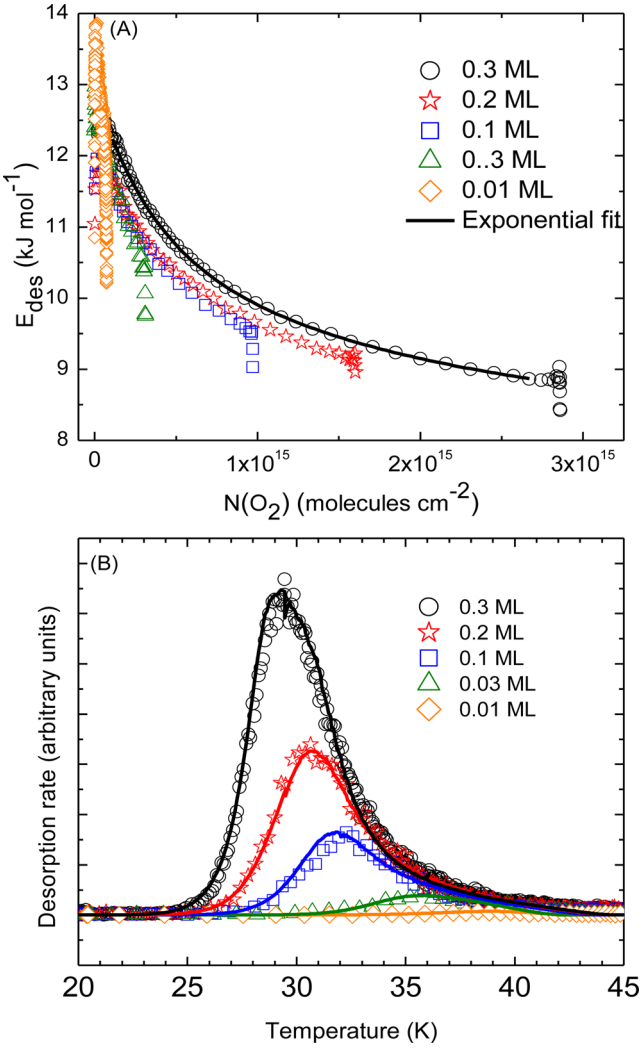

Figure 4. The top figure is the plots of E_{des} as function of N the surface concentration of adsorbed O_2 for background dosed O_2 sub-MLs. The exponential fit of the E_{des} distribution is shown for the 0.3 ML background deposition with a full line. The bottom figure is the TPD profiles of sub-ML coverages of O_2 (open symbols) on amorphous silica with the simulated curves (full lines).

H_2O molecules interact more strongly with each other than with the underlying silica, favouring the growth of islands when mobility on the silica is possible; H_2O de-wets from the silica (Kaya et al. 2007; Smith et al. 2014). In contrast, with the diatomic species, the interaction between the silica and O_2, CO, and N_2 is stronger than that between O_2 molecules; between CO molecules; and between N_2 molecules (Table 2). These species therefore wet the silica.

Table 2. E_{des} range for sub-monolayer coverages of O_2, CO and N_2 and H_2O on amorphous silica as compared to the multilayer coverage data at the bottom of the table.

Coverage / ML	E_{des} / kJ mol^{-1} (K)			
Sub-monolayer	O_2	CO	N_2	H_2O
0.01	11.0–11.9 (1320–1431)	–	–	–
0.03	10.0–11.4 (1200–1371)	10.7–12.2 (1287–1467)	11.8–13.4 (1419–1612)	–
0.06	–	9.9–11.7 (1191–1407)	10.9–12.2 (1311–1467)	–
0.1	9.0–11.2 (1100–1347)	–	–	–
0.2	8.4–11.2 (1010–1347)	–	–	38.5–41.5 (4630–4991)
0.3	8.0–11.6 (960–1395)	8.2–10.8 (986–1299)	8.8–11.2 (1058–1347)	–
0.4	–	–	–	34–36 (4090–4330)
Multilayer	O_2	CO	N_2	H_2O
≥1	7.5 ± 0.2 (902 ± 24)	7.3 ± 0.2 (878 ± 36)	6.9 ± 0.3 (830 ± 36)	49.3 ± 2 (5930 ± 240)

3.3 Vibrational spectroscopy in the sub-monolayer regime

Figs 5 and 6 present the RAIR spectra of the C–O stretching and O–H stretching regions for sub-ML quantities of CO and H_2O, respectively, on amorphous silica at 20 K. The CO spectra, with the C–O stretch at 2137 cm^{-1} (5.34 μm), show no change upon annealing the substrate from 20 to 22 and 24 K. At 26 K, CO has started to desorb and the spectrum has therefore not been included in Fig. 5. In contrast in the H_2O spectra, the O–H stretch, initially quite weak at 3239 cm^{-1} (8.10 μm), shifts and strengthens as the surface temperature is increased above 40 K until it reaches a steady state, positioned at 3252 cm^{-1} (8.13 μm), at around 100 K, with no further changes in position and intensity until H_2O desorbs from 137 K.

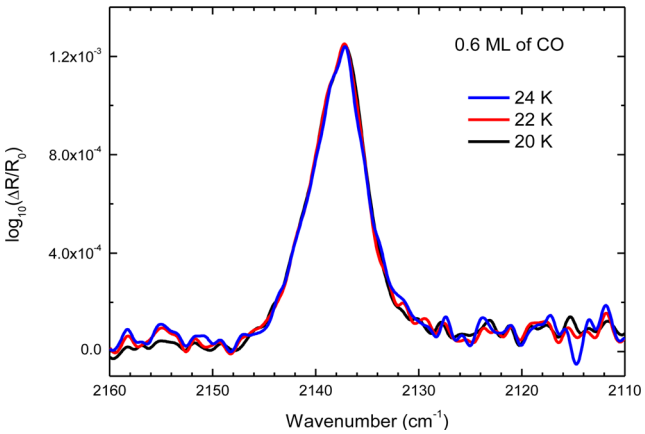

Figure 5. Temperature-programmed RAIRS of 0.6 ML CO on silica indicates no difference in the feature as the temperature is increased signifying that CO is free to diffuse above 20 K to sample the most favourable binding sites on the surface.

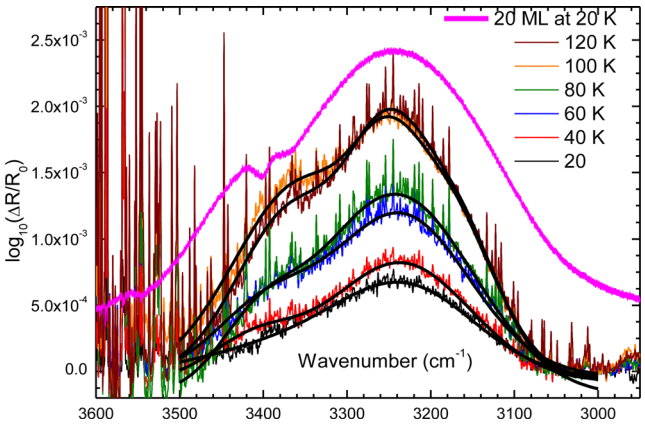

Figure 6. Temperature-programmed RAIRS of H_2O showing the diffusion of H_2O starting at about 40 K and reaching a plateau at 100 K. The dashed lines are the experimental spectra while the solid lines are a result of Gaussian fittings, meant as a guide to the eye. The 20 ML trace is scaled by a factor of 1/20 so as to compare the annealed spectra with bulk H_2O. The sharp features in the spectra are due to gas-phase H_2O present in the optics purge gas.

C–O stretching in solid CO has been extensively studied. However, as far as we are aware, the only RAIR spectra of CO on surfaces of astrophysical relevance are those reported by Collings and co-workers on water and other molecular solid surfaces (Collings et al. 2003a,b; Collings, Dever & McCoustra 2014) and Fraser and co-workers on a zeolite (Fraser et al. 2005). The position of the C–O stretch in the present data can be readily compared with the data of Collings et al. (2014). A C–O stretching feature at 2137 cm^{-1} (5.34 μm) shifted from the molecular wavenumber of 2143 cm^{-1} (5.36 μm) is entirely consistent with CO being physisorbed to the silica surface *via* its C atom in what Collings et al. describe as a σ geometry (Collings, Dever & McCoustra 2014). Pontoppidan et al. (2003) reported three features of solid CO; 2143.7 cm^{-1} (5.36 μm), 2139.9 cm^{-1} (5.35 μm) and 2136.5 cm^{-1} (5.34 μm), the first two features were ascribed to bulk CO in the ISM. The feature at 2136.5 cm^{-1} (5.34 μm) is stated as being inconsistent with what was previously thought to be a CO–H_2O interaction. The 2136.5 cm^{-1} (5.34 μm) band has also been assigned to CO mixed in methanol (CH_3OH) which is the final hydrogenation product of CO (Cuppen et al. 2011). Given the experimental uncertainties, Fig. 5 suggests an alternative assignment of CO being directly bound to the silica surface. This figure supports the assignment that the feature at 2136.5 cm^{-1} (5.34 μm) is not due to a CO–H_2O interaction. However, it is worth noting that the presence of iron and magnesium ions in the silica matrix may subtly shift this position due to modifications of the silica–CO interaction (Collings, Dever & McCoustra 2014). The invariance of the CO feature in Fig. 5 with temperature is, of course, consistent with the CO being able to readily diffuse over the silica surface to eventually sample the most energetically favourable binding sites.

The RAIR spectra of H_2O ice adsorbed on silica are less well known (Kaya et al. 2007). Indeed these data represent, to the best of our knowledge, the first measurements of H_2O sub-MLs adsorbed on silica at cryogenic temperatures. At the deposition temperature (20 K), the O–H stretch can be identified in Fig. 6 as a weak feature at 3232 cm^{-1} (8.08 μm). As we anneal, diffusion is activated at around 40 K, corresponding to a barrier height for H_2O diffusion on the silica surface of *ca.* 10–15 kJ mol^{-1} (1200–1800 K), and

island growth commences. The O–H stretch grows and shifts in intensity, from 3232 cm^{-1} (8.08 μm) to 3250 cm^{-1} (8.12 μm). In addition a new shoulder is observed to grow at 3353 cm^{-1} (8.38 μm). When the ice is annealed to 100 K and 120 K, the band resembles the RAIR spectra of 20 ML H_2O, i.e. a complete amorphous solid water film, deposited under similar conditions as shown in Fig. 6. This similarity between the annealed spectra and the bulk O–H stretching modes reflects the formation of hydrogen-bonded H_2O islands. Such behaviour is consistent with the observation that as annealing in this temperature range does not result in loss of H_2O from the surface (i.e. the number of O–H oscillators remain constant) then the intensity increase can only be due to an increase in oscillator strength. This is only known to happen with O–H stretching modes in H_2O when moving from isolated H_2O molecules to fully hydrogen-bonded H_2O molecules in bulk solid or liquid H_2O (Xantheas & Dunning 1993; Ceponkus, Uvdal & Nelander 2008). This behaviour is entirely consistent with the observed thermal desorption behaviour of H_2O on the amorphous silica surface.

4 ASTROPHYSICAL IMPLICATIONS

In the sub-ML regime, the higher energy end of the binding energy distribution in the case of all the diatomic molecules means that these molecules will have a significantly enhanced surface lifetime and so allowing them to explore the grain surface more fully. Considering a dust grain temperature of 15 K (Greenberg 1971) and increasing the binding energy of sub-ML coverages from 8.0 kJ mol^{-1} to 11.9 kJ mol^{-1} (960 to 1431 K), the range we report for the binding energy on the amorphous silica for O_2, will increase the lifetime on the surface from 23×10^6 to above 10^{20} yr. Silicate minerals in astrophysical environments are subject to radiation weathering with the consequence that in iron–magnesium silicates such as olivine, segregation of iron atoms and nanoparticles is observed (Toppani et al. 2006). A long lifetime for O_2 on such surfaces (even ignoring the likely depth of any chemisorption sites on the iron atoms and nanoparticles) will give O_2 sufficient time to explore the grain surface, find an iron atom or nanoparticle and likely undergo dissociative adsorption. Chemisorption of O_2 on iron is well known (Ertl & Huber 1980) and binding energies are typically 550 kJ mol^{-1} (66 150 K). Lifetimes of O atoms in such sites would therefore be measured on timescales of $>10^{20}$ yr at ISM temperatures. The O atoms would also be invisible to gas-phase spectroscopy, to mid-IR spectroscopy of the solid state and would be hard to distinguish from any Fe–O signatures from the mineral in the far-IR/THz. This might provide an additional sink for O in the solid state that could contribute to addressing the issue of O absence.

Water adsorbed at low temperature on silica starts diffusing around 40 K, corresponding to an activation energy of *ca.* 10–15 kJ mol^{-1} (1200–1800 K) consistent with the energy of one hydrogen-bond between H_2O and the substrate. Hence, water formed on a grain at typical dense cloud temperatures (10–15 K) would not be able to diffuse on the surface until the temperature of the dust grain is raised above 40 K by an external heat source. At the low temperatures of dense clouds, the surface of the water ice layer covering the grains is therefore static, and all water molecules formed in this environment or impinging the grains surface would freeze in their initial position, confirming the view of a ballistic deposition. A common 'rule of thumb' states that the diffusion barrier is roughly 10 per cent of the desorption energy. However, the diffusion of H_2O into islands, which desorb with zero-order kinetics and exhibit a binding energy of 35–40 kJ mol^{-1} (4210–4810 K) (consistent with two hydrogen-bonds to the H_2O surface), suggests that the binding energy of H_2O to silica would be lower. This would mean that the rule of thumb is not obeyed in this instance. The diffusion barrier of 10–15 kJ mol^{-1} (1200–1800 K) inferred in this work is much higher than what is expected from the 'rule of thumb', which would give an estimated barrier of 4 kJ mol^{-1} (480 K). The reason for the deviation in barrier energy could be that the 'rule of thumb' is more effective when considering simple van der Waals interactions as opposed to hydrogen bonding. The 15 kJ mol^{-1} (1800 K) diffusion barrier suggests that water molecules, forming at low temperatures with two hydrogen-bonds to the silica surface, have one of their hydrogen-bonds broken above 40 K. This allows diffusion, which could be pictured as a penguin-like random walk between adsorption sites, until the water molecule finds a more stable adsorption site by islanding with other water molecules. In this configuration, water molecules form on average three hydrogen-bonds, as suggested by the desorption energy of H_2O multilayers of *ca.* 50 kJ mol^{-1} (6010 K).

5 CONCLUSION

The key outcomes of this work can be summarized in a few points.

(1) Desorption of multilayer films of O_2, CO, N_2 and H_2O from the amorphous silica surface is zero order and consistent with that previously reported in the literature. The only notable exception, which is likely to have accrued from our use of line-of-sight desorption methods, is the observation of a low-temperature phase change in solid O_2 at around 25.5 K as a change of the rate of desorption. This is not unlike the behaviour observed when amorphous H_2O ice crystallizes.

(2) In the sub-ML regime, distinctly contrasting behaviour is seen from the diatomic molecules and H_2O. The diatomic species explore the range of binding sites on the amorphous silica surface, finding the energetically most favourable sites and consequently desorbing with first-order kinetics. O_2, N_2 and CO clearly wet the silica surface. Binding energy data are presented which support this assertion. In the case of H_2O, the H_2O–H_2O interactions dominate over the H_2O–silica interactions and even at the lowest of coverages studied, H_2O film growth follows an island growth model and zero-order desorption kinetics. H_2O therefore de-wets from the silica surface at temperatures significantly below the desorption temperature.

(3) CO RAIR spectra in the sub-ML regime are consistent with adsorption in a geometry where CO interacts with the silica surface *via* its C atom in what Collings et al. (2014) describe as a σ geometry. The shift in frequency from gaseous CO is consistent with the strength of interaction in the sub-ML regime extracted from inversion of the relevant TPD data.

(4) H_2O RAIR spectra for sub-ML coverages on amorphous silica at temperatures below 30 K confirm the ballistic deposition mechanism that many have postulated for growth in this temperature regime (Zondlo et al. 1997; Kimmel et al. 2001). At temperatures above 40 K, the weak O–H stretching spectra strengthen in a manner consistent with increasing ease of diffusion and growth of H_2O cluster and islands. This we believe is the first observation of such and suggests that H_2O diffusion is thermally activated above 40 K.

Our results have astrophysical implications for gas–grain exchanges in the dense and diffuse ISM clouds. The morphology of the dust grains surface seems to exert a non-negligible influence on desorption of adsorbed species by offering binding sites with a range of binding energies. Higher desorption energies in the sub-ML

regime mean a higher lifetime for the molecules adsorbed on bare silica at the edge of the molecular clouds and proto-planetary discs. They could be more efficiently processed by UV and higher energy photons or by reactive radicals and give rise to a specific chemistry for the molecular species in this low H_2O concentration. The multilayer studies of O_2 might also suggest that a part of the apparent 'oxygen budget reduction' could be due to the underestimation of the solid O_2 abundance on ices.

More importantly we have established that sub-ML TPD and RAIRS studies, especially on CO and H_2O, will allow us to probe the physicochemical nature of more realistic silicate surface models containing iron and magnesium; especially under conditions where metallic segregation may be promoted by ionizing radiation exposure.

ACKNOWLEDGEMENTS

The authors acknowledge the support of the UK Engineering and Physical Science Research Council (EPSRC, EP/D506158/1) and the European Community FP7-ITN Marie-Curie Programme (LASSIE project, grant agreement #238258). VLF thanks EPSRC for a DTA Studentship; Ryan Nish (Heriot-Watt University chemistry undergraduate project student), Ellen Kendrick and Sandy Watt (Nuffield Foundation project students) for their assistance in the experiments. ARF thanks HWU for a James Watt Scholarship. JL and DM acknowledge funding from the European Community FP7-ITN Marie-Curie Programme (LASSIE project, grant agreement #238258). The authors also acknowledge Dr. Ali G. M. Abdulgalil for his valuable experimental assistance.

REFERENCES

Acharyya K., Fuchs G. W., Fraser H. J., van Dishoeck E. F., Linnartz H., 2007, A&A, 466, 1005
Bar-Nun A., Herman G., Laufer D., Rappaport M. L., 1985, Icarus, 63, 317
Belloche A., Andre P., 2004, A&A, 419, L35
Bergin E. A., Alves J., Huard T., Lada C. J., 2002, ApJ, 570, L101
Bisschop S. E., Fraser H. J., Öberg K. I., van Dishoeck E. F., Schlemmer S., 2006, A&A, 449, 1297
Bolina A. S., Wolff A. J., Brown W. A., 2005, J. Phys. Chem. B, 109, 16836
Cairns B. R., Pimentel G. C., 1965, J. Chem. Phys., 43, 3432
Ceponkus J., Uvdal P., Nelander B., 2008, J. Phys. Chem. A, 112, 3921
Chiar J. E., Gerakines P. A., Whittet D. C. B., Pendleton Y. J., Tielens A. G. G. M., Adamson A. J., Boogert A. C. A., 1998, ApJ, 498, 716
Collings M. P., Dever J. W., Fraser H. J., McCoustra M. R. S., 2003a, Ap&SS, 285, 633
Collings M. P., Dever J. W., Fraser H. J., McCoustra M. R. S., Williams D. A., 2003b, ApJ, 583, 1058
Collings M. P., Anderson M. A., Chen R., Dever J. W., Viti S., Williams D. A., McCoustra M. R. S., 2004, MNRAS, 354, 1133
Collings M. P., Dever J. W., McCoustra M. R. S., 2014, Phys. Chem. Chem. Phys., 16, 3479
Cuppen H. M., Penteado E. M., Isokoski K., van der Marel N., Linnartz H., 2011, MNRAS, 417, 2809
Dulieu F., Congiu E., Noble J., Baouche S., Chaabouni H., Moudens A., Minisalle M., Cazaux S., 2013, Sci. Rep., 3, 1338
Ehrenfreund P., Charnley S. B., 2000, ARA&A, 38, 427
Ertl G., Huber M., 1980, Z. Phys. Chem., 119, 97
Fraser H. J., Collings M. P., McCoustra M. R. S., Williams D. A., 2001, MNRAS, 327, 1165
Fraser H. J., Collings M. P., McCoustra M. R. S., 2002, Rev. Sci. Instrum., 73, 2161
Fraser H. J., Bisschop S. E., Pontoppidan K. M., Tielens A. G. G. M., van Dishoeck E. F., 2005, MNRAS, 356, 1283
Freiman Y. A., Jodl H. J., 2004, Phys. Rep., 401, 1
Fuchs G. W. et al., 2006, Faraday Discussion, 133, 331
Garrod R., Park I. H., Caselli P., Herbst E., 2006, Faraday Discuss., 133, 51
Gill E. K., Morrison J. A., 1966, J. Chem. Phys., 45, 1585
Gillet F. C., Forrest W. J., 1973, ApJ, 483
Goldsmith P. F. et al., 2000, ApJ, 539, L123
Green S. D., Chen R., Collings M. P., Brown W. A., McCoustra M. R. S., 2009, MNRAS, 398, 357
Greenberg J. M., 1971, A&A, 12, 240
Haq S., Harnett J., Hodgson A., 2002, Surf. Sci., 505, 171
Hincelin U., Wakelam V., Hersant F., Guilloteau S., Loison J. C., Honvault P., Troe J., 2011, A&A, 530, A61
Hollenbach D., Kaufman M. J., Bergin E. A., Melnick G. J., 2009, ApJ, 690, 1497
Jenkins E. B., 2009, ApJ, 700, 1299
Jenniskens P., Blake D. F., 1994, Science, 265, 753
Jenniskens P., Blake D. F., Wilson M. A., Pohorille A., 1995, ApJ, 455, 389
Kaya S., Weissenrieder J., Stacchiola D., Shaikhutdinov S., Freund H. -J., 2007, J. Phys. Chem. C, 111, 759
Kimmel G. A., Dohnálek Z., Stevenson K. P., Smith R. S., Kay B. D., 2001, J. Chem. Phys., 114, 5295
King D. A., 1975, Surf. Sci., 47, 384
Larsson B. et al., 2007, A&A, 466, 999
Liseau R. et al., 2012, A&A, 541, A73
Liszt H. S., 2007, A&A, 476, 291
Lu Q.-B., Madey T. U., Parenteau L., Weik F., Sanche L., 2001, Chem. Phys. Lett., 342, 1
Meyer D. M., Cardelli J. A., Sophia U. J., 1997, ApJ, 490, L103
Meyer D. M., Jura M., Cardelli J. A., 1998, ApJ, 493, 222
Narten A. H., Venkatesh C. G., Rice S. A., 1976, J. Chem. Phys., 64, 1106
Noble J. A., Congiu E., Dulieu F., Fraser H. J., 2012, MNRAS, 4, 768
Öberg K. I., van Broekhuizen F., Fraser H. J., Bisschop S. E., van Dishoeck E. F., Schlemmer S., 2005, ApJ, 621, L33
Onaka T., Okada Y., 2003, ApJ, 585, 872
O'Neill P. T., Williams D. A., 1999, Ap&SS, 266, 539
Pontoppidan K. M. et al., 2003, A&A, 408, 981
Pontoppidan K. M., van Dishoeck E. F., Dartois E., 2004, A&A, 426, 925
Sandqvist Aa. et al., 2008, A&A, 482, 849
Smith R. S., Huang C., Wong E. K. L., Kay B. D., 1997, Phys. Rev. Lett., 79, 909
Smith R. S., Scott R., Matthiesen J., Kay B. D., 2014, J. Phys. Chem. A, 118, 8242
Stevens K. P., Kimmel G. A., Donhalek Z., Smith R. S., Kay B. D., 1999, Science, 283, 1505
Tait S. L., Dohnalek Z., Campbell C. T., Kay B. D., 2005, J. Chem. Phys., 122, 164707
Thi W. -F., van Dishoeck E. F., Pontoppidan K. M., Dartois E., 2010, MNRAS, 406, 1409
Thrower J. D., Collings M. P., Rutten F. J. M., McCoustra M. R. S., 2009a, J. Chem. Phys., 131, 244711
Thrower J. D., Collings M. P., Rutten F. J. M., McCoustra M. R. S., 2009b, MNRAS, 394, 1510
Thrower J. D., 2009c, PhD thesis, Heriot-Watt University
Tielens A. G. G. M., 2005, The Physics and Chemistry of the Interstellar Medium, Cambridge Univ. Press, Cambridge
Tielens A. G. G. M., 2013, Rev. Mod. Phys., 85, 1021
Toppani A., Dukes C., Baragiola R., Bradley J. P., 2006, Lunar Planet. Sci., 37, 2056
van Dishoeck E. F., Phillips T. G., Keene J., Blake G. A., 1992, A&A, 261, L13
Westphal A. J. et al., 2014, Science, 345, 786
Whittet D. C. B., 2010, ApJ, 710, 1009
Williams D. A., Taylor S. D., 1996, Q. J. R. Astron. Soc., 37, 565
Xantheas S. S., Dunning T. H., Jr, 1993, J. Chem. Phys., 99, 8774
Zondlo M. A., Onasch T. B., Warshawsky M. S., Tolbert M. A., Mallick G., Arentz P., Robinson M. S., 1997, J. Phys. Chem. B, 101, 1088

This paper has been typeset from a TEX/LATEX file prepared by the author.